

Signal Subgraph Estimation Via Vertex Screening

Shangsi Wang, Cencheng Shen, Alexandra Badea, Carey E. Priebe, Joshua T. Vogelstein

Abstract—Graph classification and regression have wide applications in a variety of domains. A graph is a complex and high-dimensional object, which poses great challenges to traditional machine learning algorithms. Accurately and efficiently locating a small signal subgraph dependent on the label of interest can dramatically improve the performance of subsequent statistical inference. Moreover, estimating a signal subgraph can aid humans with interpreting these results. We present a vertex screening method to identify the signal subgraph when given multiple graphs and associated labels. The method utilizes distance-based correlation to screen the vertices, and allows the subsequent classification and regression to be performed on a small induced subgraph. We demonstrate that this method is consistent in recovering signal vertices and leads to better classification performance via theory and numerical experiments. We apply the vertex screening algorithm on human and murine graphs derived from functional and structural magnetic resonance images to analyze the site effects and sex differences.

Index Terms—multiple graphs, iterative screening, distance correlation, graph classification

1 INTRODUCTION

Graph classification and regression are crucial to analyze data sets in various fields such as neuroscience, internet mapping, and social networks [1]–[3]. Given a set of graphs $\{G_i\}_{i=1}^m$ along with a set of corresponding covariates $\{Y_i\}_{i=1}^m$, we would like to predict the covariate Y_i based on the graph G_i . However, G can be extremely large in practice, e.g., the social networks and raw neuroimages can have millions of vertices [4], which is a great challenge computationally without first reducing the size of the graph. Therefore, it is imperative to come up with an accurate and efficient method for signal subgraph estimation. Signal subgraph extraction tries to locate a subgraph of G that contains all the useful information about Y , which can be helpful to improve the subsequent inference performance. However, estimating the signal subgraph is very challenging for large graphs, because a graph with n vertices could have 2^n different induced subgraphs.

When the number of features is large, dimension reduction and feature selection is generally difficult and expen-

sive, which is a challenge to many modern real data sets. To overcome this challenge, Fan and Lv [5] proposed the feature screening algorithm and showed that ranking variables via the Pearson's correlation possesses a sure screening property under linear regression models. Screening through marginal likelihood are later considered for generalized linear models [6], [7]. Motivated by their approaches, we develop a vertex screening procedure to estimate the signal subgraph.

To screen the vertices effectively requires a sufficient measure of "correlation". Although Pearson's product moment correlation has been a popular choice, it only captures linear association and thus is not a good candidate for identifying general dependencies. The recently proposed distance correlation (Dcorr) [8]–[10] is able to detect all types of dependencies between two random variables consistently. The later proposed multiscale generalize correlation (MGC) [11]–[13] is a localized version of Dcorr, which shares the consistency property with improved finite-sample testing power against nonlinear dependencies. For a review of Dcorr and MGC, please see Appendices. Consistent screening under a model-free setting via distance correlation was proposed and investigated in [14], [15].

We therefore combine distance-based correlation and screening to yield an effective vertex screening method to estimate the signal subgraph, which works efficiently and tackles all inherent challenges. The methodology consists of three steps: (i) feature computation, (ii) calculating the distance-based correlation, and (iii) thresholding. The first step computes a feature for each vertex based the graph. The second step calculates a distance-based correlation measure between the feature of each vertex and the label of interest Y over all graphs. The last step thresholds the correlations and only keeps the vertices with large correlations. We further developed an iterative vertex screening algorithm, in which the three steps are applied recursively to improve the performance without sacrificing the running time. In the next

- Shangsi Wang and Carey Priebe are with the Department of Applied Mathematics and Statistics, Johns Hopkins University. E-mail: swang127@jhu.edu, cep@jhu.edu
- Cencheng Shen is with the Center for Imaging Science, Johns Hopkins University; Joshua Vogelstein is with the Center for Imaging Science, Department of Biomedical Engineering and Institute for Computational Medicine, Johns Hopkins University. E-mail: cshen6@jhu.edu, jovo@jhu.edu
- Alexandra Badea is with Center for In Vivo Microscopy, Duke University Medical Center. E-mail: alexandra.badea@duke.edu
- The authors gratefully acknowledge support from the Defense Advanced Research Projects Agency's (DARPA) GRAPHs program through contract N66001-14-1-4028, the DARPA SIMPLEX program through contract N66001-15-C-4041, the DARPA D3M program through contract FA8750-17-2-0112, and the National Science Foundation Division of Mathematical Sciences award DMS-1712947. This work is also supported in part by the National Institutes of Health through K01 AG041211, R01 AG045422, R56 AG051765, P41 EB015897 and S10OD010683. The authors would like to thank Dr. Daniel S. Margulies provided useful feedback.

section, we introduce the signal graph estimation problem. In the Main Result Section, we present our algorithm and theoretical properties of the algorithm. In the Experiments Section, we demonstrate the utility of the algorithm through a series of experiments. Finally, we conclude the paper with a discussion about possible future extensions.

2 PRELIMINARIES

2.1 Setting

Given m graphs $\{G_i, i = 1, \dots, m\}$ with a shared vertex set $V = [n]$, let $A_i \in \mathbb{R}^{n \times n}$ be the adjacency matrix of G_i for each i , which can be weighted or un-weighted, directed or un-directed. Additionally, there is a covariate of interest $\{Y_i \in \mathbb{R}, i = 1, \dots, m\}$ associated to each graph. A common example is in neuroimage study, where the human brain image of a subject is G_i , and the phenotype of the subject is Y_i . The brain versus phenotype pair is collected for m subjects. In this paper, we focus on the case that Y_i is a scalar label, but the screening algorithm is readily applicable to any multivariate Y_i . The classical statistical pattern recognition set up is that $\{(G_i, Y_i)\}_{i=1}^m$ are independent and identically distributed pairs according to some distribution $F_{G,Y}$ [16], that is

$$(G_1, Y_1), (G_2, Y_2), (G_3, Y_3), \dots, (G_m, Y_m) \stackrel{i.i.d.}{\sim} F_{G,Y}$$

for some true but unknown joint distribution.

It is often the case that the covariate Y only depends on a small part of G . In addition, merely predicting Y is insufficient in some applications. It is desirable to know which vertices or subgraph is associated to Y . Therefore, it is natural to search for a signal subgraph such that Y is independent of other parts of the graph. This motivates our definition of signal vertices and signal subgraph.

Definition For any subset of vertices $U \subset V = [n]$, denote the induced subgraph of U by $G[U]$, and denote the subgraph removing all edges in $G[U]$ as $G \setminus G[U]$.

The set of *signal vertices* S is defined to be the minimal subset of vertices U , such that $G \setminus G[U]$ is independent of Y , that is

$$S = \arg \min_U |U|, \text{ subject to } G \setminus G[U] \perp Y,$$

where the notation \perp means independence, or $F_{G \setminus G[U], Y} = F_{G \setminus G[U]} F_Y$. The induced graph $G[S]$ on the signal vertices is called the *signal subgraph*.

If the graph G is independent of Y , there is no signal in the graph and the signal subgraph is empty in this case. If all vertices in G are incident on at least one edge which is dependent on Y , the signal subgraph is the whole graph G . Moreover, there can be multiple subsets attaining the minimum, so for ease of presentation we assume there exists a unique signal subgraph $G[S]$.

In practice, m graph-covariate pairs $\{(A_i, Y_i)\}_{i=1}^m$ are observed, we want to estimate the signal subgraph $G[S]$. The subsequent statistical inference can benefit from the bias-variance trade-off or statistical parsimony, if vertices with weak or no signal can be screened out effectively.

2.2 Graph Classification

We introduce a binary classification problem that is predicting the label $Y \in \{0, 1\}$ using graph G , which serves as the foundation for Section 3.4 and later simulations.

The network model under consideration is the inhomogeneous Erdos-Renyi (IER) random graph model [17]. It generalizes the well known Erdos-Renyi model to allow edge to have different probability and gives rises to a family of distribution on undirected graphs. IER model can also be understood as a stochastic block model with each block having only one vertex [18].

Definition Inhomogeneous Erdos-Renyi model (IER). A random adjacency matrix A is said to follow an inhomogeneous Erdos-Renyi random graph model with edge probability matrix $P \in [0, 1]^{n \times n}$, if the edge probability between vertex u and v is $P[u, v]$ and independent of other edges. The notation is $A \sim IER(P)$, and the likelihood of A under this model is

$$\mathcal{L}(A; P) = \prod_{u < v} (P[u, v])^{A[u, v]} (1 - P[u, v])^{1 - A[u, v]}.$$

The class label is built into this model as follows: suppose the graph follow IER model conditioned on Y , that is

$$A|Y = y \sim IER(P^y) \quad \text{for } y \in \{0, 1\}.$$

Under this setting, it is clear that vertex u is a signal vertex if and only if $P^0[u, v] \neq P^1[u, v]$ for some vertex v , that is

$$S = \{u \in V | \exists v \in V, P^0[u, v] \neq P^1[u, v]\}.$$

Given this model, it is known that the optimal classification performance is achieved by the Bayes classifier g^* [16], which is defined

$$g^*(A) = \begin{cases} 1 & \text{if } \pi_0 \mathcal{L}(A; P^0) < \pi_1 \mathcal{L}(A; P^1), \\ 0 & \text{if } \pi_0 \mathcal{L}(A; P^0) \geq \pi_1 \mathcal{L}(A; P^1), \end{cases}$$

where π_0 and π_1 are prior probabilities for each class. In practice, it is natural to consider the Bayes plug-in classifier which estimates the π_y and P^y and plug them into the likelihood. In this case, the maximum likelihood estimates of parameters are

$$\hat{\pi}_y = \frac{\sum_i \mathbb{I}\{Y_i = y\}}{m},$$

$$\hat{P}^y = \frac{\sum_i \mathbb{I}\{Y_i = y\} A_i}{\sum_i \mathbb{I}\{Y_i = y\}}.$$

Using these estimates, we can construct the Bayes plug-in classifier g_V based on the whole graph, that is

$$g_V(A) = \begin{cases} 1 & \text{if } \hat{\pi}_0 \mathcal{L}(A; \hat{P}^0) < \hat{\pi}_1 \mathcal{L}(A; \hat{P}^1), \\ 0 & \text{if } \hat{\pi}_0 \mathcal{L}(A; \hat{P}^0) \geq \hat{\pi}_1 \mathcal{L}(A; \hat{P}^1). \end{cases}$$

When we have an estimate of the signal subgraph $G[\hat{S}]$, we could also consider Bayes plug-in classifier $g_{\hat{S}}$ based on the estimated signal subgraph, that is

$$g_{\hat{S}}(A) = \begin{cases} 1 & \text{if } \hat{\pi}_0 \mathcal{L}(A[\hat{S}]; \hat{P}^0[\hat{S}]) < \hat{\pi}_1 \mathcal{L}(A[\hat{S}]; \hat{P}^1[\hat{S}]), \\ 0 & \text{if } \hat{\pi}_0 \mathcal{L}(A[\hat{S}]; \hat{P}^0[\hat{S}]) \geq \hat{\pi}_1 \mathcal{L}(A[\hat{S}]; \hat{P}^1[\hat{S}]), \end{cases}$$

where

$$\mathcal{L}(A[\hat{S}]; \hat{P}^y[\hat{S}]) = \prod_{u, v \in \hat{S}} A[u, v]^{\hat{P}^y[u, v]} (1 - A[u, v])^{(1 - \hat{P}^y[u, v])}.$$

Similarly, we use g_S to denote the Bayes plug-in classifier based on the true signal subgraph.

To evaluate the classification performance, we consider the $0 - 1$ loss or classification error L . For a classifier g , the loss $L(g)$ is defined by

$$L(g) = \mathbb{P}(g(A) \neq Y).$$

In Section 3.4, we investigate how $L(g_V)$ and $L(g_S)$ behave, i.e., the classification error based on the full graph versus the classification error based on the estimated signal subgraph.

3 METHOD AND THEORY

3.1 Main Algorithm

The vertex screening procedure provides an estimate of signal subgraph $G[\hat{S}]$ via the following steps: feature extraction, distance-based correlation computation and thresholding. We also develop an iterative vertex screening procedure, which applies the three steps recursively. We will first present the non-iterative vertex screening, followed by the iterative version.

The first step extracts a feature vector for each vertex in a graph. We use the notation $\hat{X}_i[u, \cdot]$ to denote the feature extracted for vertex u in graph i where $i \in [m]$ and $u \in [n]$. A simple example is setting $\hat{X}_i[u, \cdot]$ to be the u th row of adjacency matrix A_i , that is $\hat{X}_i[u, \cdot] = A_i[u, \cdot]$. As a result, $\hat{X}_i[u, \cdot]$ is a vector in \mathbb{R}^n which can be a high dimensional space. Alternatively, summary statistics can be treated as a feature vector. For example, the number of vertices within k -neighborhood of the vertex or eccentricity of the vertex can be used as the feature for the vertex [19], [20]. Spectral methods could also be applied to extract a feature vector which lies in \mathbb{R}^d . For example, Adjacency Spectral Embedding [18] and Joint Embedding [21] could recover a low dimension latent position for each vertex. In this paper, we focus on using adjacency vector as the vertex feature for simplicity.

The second step computes sample distance-based correlation between the feature vector $\{\hat{X}_i[u, \cdot]\}_{i=1}^m$ and label $\{Y_i\}_{i=1}^m$ for each vertex $u \in V$. The correlation choice is either distance correlation (Dcorr) or multiscale generalized correlation (MGC). Denote the distance-based correlation by c_u , that is

$$c_u = \text{Dcorr}(\{\hat{X}_i[u, \cdot], Y_i\}_{i=1}^m), \text{ or}$$

$$c_u = \text{MGC}(\{\hat{X}_i[u, \cdot], Y_i\}_{i=1}^m).$$

The motivation of Dcorr and MGC is that they can detect any kind of dependency when the sample size is large enough. Generally speaking, we recommend using MGC when m is small but to use Dcorr when m is large. This is because Dcorr runs in $\mathcal{O}(m^2n)$ while MGC runs in $\mathcal{O}(m^2n \log(m))$. Then for small m , the computation difference is negligible while MGC can be more powerful against general dependencies; while for m large (like above 1000 graphs) the power difference is negligible against most dependencies due to the consistency, and Dcorr wins in the running time.

The last step orders $\{c_u\}_{u \in V}$ by their magnitudes, and we threshold the correlations by a critical value c . The

vertices surviving the threshold are the estimated signal vertices \hat{S} , that is

$$\hat{S} = \{u \in V | c_u > c\}.$$

The estimated signal subgraph and the corresponding adjacency matrix are denoted by $G[\hat{S}]$ and $A[\hat{S}]$ respectively. Algorithm 1 describes the general procedure of vertex screening using adjacency vector as the feature vector.

Algorithm 1 Vertex Screening.

Require: $\{(A_i, Y_i)\}_{i=1}^m$ and $c \in [0, 1]$

1: **for** $u \in V$ **do**
2: $c_u = \text{Dcorr}(\{(A_i[u, \cdot], Y_i)\}_{i=1}^m)$
3: **end for**
4: $\hat{S} = \{u \in V | c_u > c\}.$

We observe that vertex feature vector $\hat{X}_i[u, \cdot]$ has dimension n , which is the number of vertices. If the vertex screening is performed on a smaller graph, $\hat{X}_i[u, \cdot]$ has fewer dimension and is more likely to exhibit a stronger signal via a larger distance-based correlation statistic with Y_i for a signal vertex. This observation motivates the iterative version that repeatedly applies Algorithm 1, i.e., at each iteration, only a small proportion δ of all vertices are removed from the graph. The size of the subgraph is iteratively reduced until size 1 or some pre-determined number. Among all possible subgraphs, pick the subgraph that has the largest Dcorr or MGC statistic with the class label. The details are described by Algorithm 2, where $A_i[V_k]$ denotes the adjacency matrix of V_k induced subgraph of graph i .

Alternatively, other possible methods to select the subgraph include: 1) use cross-validation [22] to select the size of the subgraph with the best leave-one-out prediction error, which can be computationally expensive; 2) order the correlations $\{c_u\}_{u \in V}$ to locate a gap among correlations, and select the vertices larger than this gap [23]; 3) background information available could determine the number of vertices which could have signal. In the experiment section, we will verify the iterative screening method that maximizes the statistics, which works very well and almost always achieves the best leave-one-out prediction error.

Note that the iterative algorithm circumvents choosing the threshold c by designating a δ . For large graphs, empirically it suffices to let δ be 0.5, which achieves an excellent performance with only a $\log(n)$ factor increase in running time. For graphs with a small number of vertices, the running time is not a issue; one may let δ be 0.05 or even reduce the size of subgraph by 1 in each iteration.

3.2 Screening Theory

The next theorem states that if the threshold t is small enough to make sure $|\hat{S}| > |S|$, then \hat{S} contains S with high probability as the number graphs increases. This theorem is a direct consequence of Theorem 1 by Li, Zhong and Zhu [15].

Theorem 3.1. If the following condition is satisfied

$$\min Dcorr(A[u, \cdot], Y) \geq c > 0 \quad \text{for } u \in S,$$

Algorithm 2 Iterative Vertex Screening.

Require: $\{(A_i, Y_i)\}_{i=1}^m, \delta \in (0, 1)$

- 1: Set $k = 1$, and $V_k = V$
- 2: **while** $|V_k| > 1$ **do**
- 3: **for** $u \in V_k$ **do**
- 4: $c_u = Dcorr(\{(A_i^{V_k}[u, \cdot], Y_i)\}_{i=1}^m)$
- 5: **end for**
- 6: Set t_k be the δ quantile among $\{c_u, u \in V_k\}$
- 7: Set $V_{k+1} = \{u \in V_k | c_u > t_k\}$
- 8: Set $k = k + 1$
- 9: **end while**
- 10: $k^* = \arg \max_k Dcorr(\{(A_i^{V_k}[V_k, \cdot], Y_i)\}_{i=1}^m)$
- 11: Output the signal vertices $\hat{S} = V_{k^*}$.

then \hat{S} contains S with high probability. Specifically, there exist two constants $c_1, c_2 > 0$, for any $0 < \gamma < 1/2$,

$$P(S \subset \hat{S}) > 1 - O(n \exp(-c_1 m^{1-2\gamma}) + n^2 \exp(-c_2 m^\gamma)).$$

The theorem states that the estimated signal subgraph contains the true signal subgraph with high probability. Actually, it is also possible to derive a threshold t to ensure $P(S = \hat{S})$ as the number of graphs goes to infinity. For the proof of Theorem 3.1, please refer to Theorem 1 in [15]. Similar results also hold for MGC [12].

3.3 Justification on Iterative Screening

Despite the consistency of screening proven above, the finite-sample performance for non-iterative screening can be often improved by iterative screening. The next theorem justifies this phenomenon, which demonstrates that the signal vertices will have its signal amplified under distance correlation by eliminating the noise vertices.

To simplify the discussion, we assume the feature vector X consists of two sets of entries that is $X = [X^*, Z]$, where $X^* \in \mathbb{R}^p$ and $Z \in \mathbb{R}^r$. Suppose X^* is the true signal and is dependent on Y , while Z is noise and is independent of Y and X^* . The first Lemma claims that the distance covariance between X and Y increases after removing the noise entries Z .

Lemma 3.2. Suppose that $X = [X^*, Z] \in \mathbb{R}^p \times \mathbb{R}^r$, where $X^* \not\perp Y, Z \perp Y$, and $Z \perp X^*$. Then,

$$Dcov(X^*, Y) \geq Dcov(X, Y).$$

If we let r increase by adding more noise entries to X , the next theorem claims that the distance correlation will decrease to 0 as r goes to infinity.

Theorem 3.3. Suppose that $X_r = [X^*, Z_r] \in \mathbb{R}^p \times \mathbb{R}^r$, where $X^* \not\perp Y, Z_r \perp Y$, and $Z_r \perp X^*$. Assume $Z_r \in \mathbb{R}^r$ has independent and identically distributed entries, then

$$\lim_{r \rightarrow \infty} Dcorr(X_r, Y) = 0.$$

Therefore, if the screening algorithm iteratively eliminates the noise vertices, the distance correlation between the signal vertex and label will become larger and larger. As a result, iterative screening can provide a more accurate ranking of signal vertices than one-time screening.

3.4 Classification Improvement

The last theoretical piece is to show that the estimated signal subgraph indeed improves the classification performance. Let e denote the number of possible edges on the graph (which is $O(n^2)$ for dense graphs), and denote the minimum of class priors by α , that is $\alpha = \min\{\pi_0, \pi_1\}$. We first analyze the performance of Bayes plug-in classifier based on the whole graph g_V . The next theorem states that its prediction error $L(g_V)$ converges to the Bayes optimal error $L(g^*)$ as the number of graphs goes to infinity.

Theorem 3.4. With high probability, $L(g_V) - L(g^*)$ is bounded by ϵ , that is

$$\mathbb{P}(L(g_V) - L(g^*) < \epsilon) \geq 1 - 2(e+1) \exp\left(\frac{-m\alpha\epsilon^2}{(2e + \sqrt{2\alpha})^2}\right).$$

Alternatively, with probability at least $1 - \eta$

$$L(g_V) - L(g^*) \leq (2e + \sqrt{2\alpha}) \sqrt{\frac{\log(\frac{2(e+1)}{\eta})}{m\alpha}}.$$

Corollary 3.5. For small $\epsilon > 0$,

$$\mathbb{E}(L(g_V)) \leq L(g^*) + \epsilon + 2(e+1) \exp\left(\frac{-m\alpha\epsilon^2}{(2e + \sqrt{2\alpha})^2}\right).$$

The theorem and corollary above consider predicting Y based on the whole graph. If we first apply vertex screening and then predict Y based on estimated signal subgraph \hat{S} using the Bayes plug-in classifier, we will have the following results by applying Theorem 3.1.

Theorem 3.6. With high probability, $L(g_{\hat{S}}) - L(g^*)$ is bounded by ϵ . Specifically, there exist constants c_1, c_2 , and c_3 , such that

$$\mathbb{P}(L(g_{\hat{S}}) - L(g^*) < \epsilon) \geq 1 - 2(e_s + 1) \exp\left(\frac{-m\alpha\epsilon^2}{(2e_s + \sqrt{2\alpha})^2}\right) - c_3(n \exp(-c_1 m^{\frac{1}{3}}) + n^2 \exp(-c_2 m^{\frac{1}{3}})),$$

where e_s is the number of possible edges in the estimated signal subgraph.

Corollary 3.7. For any $\epsilon > 0$, there exist three constants c_1, c_2 and c_3 ,

$$\begin{aligned} \mathbb{E}(L(g_{\hat{S}})) &< L(g^*) + \epsilon \\ &+ 2(e_s + 1) \exp\left(\frac{-m\alpha\epsilon^2}{(2e_s + \sqrt{2\alpha})^2}\right) \\ &+ c_3(n \exp(-c_1 m^{\frac{1}{3}}) + n^2 \exp(-c_2 m^{\frac{1}{3}})). \end{aligned}$$

Comparing Theorem 3.2 and 3.4, we can see that if $n, |S|$ and $|\hat{S}|$ are fixed, $L(g_V)$ and $L(g_{\hat{S}})$ are both converging to $L(g^*)$ with m going to infinity. In fact, prediction based on the whole graph converges at a faster rate to the Bayes optimal. If $n, |S|$ and $|\hat{S}|$ increase faster than $m^{\frac{1}{2}}$, then both prediction with or without screening have no error bound guarantees. However, if $|S|$ and $|\hat{S}|$ are fixed and n grow faster than $m^{\frac{1}{2}}$, only vertex screening guarantees convergence of prediction error. We state this in the next theorem.

Theorem 3.8. Assume $|S|$ and $|\hat{S}|$ are fixed, and $n \in O(\exp(m^{\frac{1}{6}}))$ and $m \in o(n^2)$, then $L(g_{\hat{S}}) \rightarrow L(g^*)$, while $L(g_V)$ is not guaranteed to converge to the Bayes optimal error.

This justifies the importance of estimating the signal subgraph in classification.

4 EXPERIMENTS

4.1 Experiment 1: Vertex Screening under IER

In this experiment, we investigate the performance of vertex screening under various setting. We generate 100 graphs from 2 classes, that is $A|Y = y \sim IER(P^y)$ with $y \in \{0, 1\}$ and

$$P^y = \begin{bmatrix} p^y \times \mathbf{1}_{20 \times 20} & 0.2 \times \mathbf{1}_{20 \times 180} \\ 0.2 \times \mathbf{1}_{180 \times 20} & 0.3 \times \mathbf{1}_{180 \times 180} \end{bmatrix},$$

where $p^0 = 0.3$ and $p^1 = 0.4$. Based on this data generation scheme, each graph has 200 vertices with the first 20 vertices being the signal vertices. Note that it is also equivalent to generating graphs from two Stochastic Block models [18], where the vertices in the first block are signal vertices.

We carry out the one-time screening using Dcorr and MGC, iterative screening (ItDcorr and ItMGC) with δ being 0.5 and 0.05 respectively. As the true signal subgraph size is 20, all the screening methods are required to return the estimated signal subgraph with 20 vertices. For comparison, screening with canonical correlation analysis (CCA) [24] and RV coefficient (RV) [25] are also included. We repeat the data generation and screening 100 times. Figure 1 shows the Receiver operating characteristic (ROC) [26] of one repeat. In this experiment, screening with Dcorr and MGC always yields similar results, so only MGC is shown in Figure 1. Table 1 reports the area under the curve (AUC) [27]

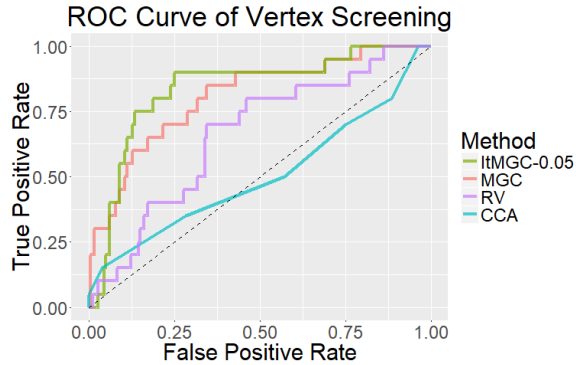


Figure 1: Receiver operating characteristic of four vertex screening procedures. The graphs are generated as described in Section 4.1. In terms of AUC, distance based screening methods perform better than RV and CCA under this setup. Iterative vertex screening is also better than one-time vertex screening.

for all methods along with the running time. We observe that Dcorr and MGC work much better than CCA and RV, iterative screening at $\delta = 0.5$ improves the performance further with a slight increase of running time, while iterative screening at $\delta = 0.05$ improves marginally at the cost of much higher running time.

Method	AUC	Time (sec)
ItDcorr-0.05	0.8605 (0.0103)	14.50 (1.45)
ItDcorr-0.50	0.8455 (0.0091)	1.73 (0.19)
ItMGC-0.05	0.8620 (0.0116)	856.37 (14.45)
ItMGC-0.50	0.8425 (0.0120)	110.23 (7.19)
Dcorr	0.8262 (0.0056)	1.20 (0.18)
MGC	0.8241 (0.0057)	33.39 (1.90)
RV	0.7074 (0.0077)	1.99 (0.09)
CCA	0.5353 (0.0080)	0.8 (0.05)

TABLE 1: The mean and standard error of AUC and running time of the eight vertex screening approaches across 100 repeats. Iterative vertex screening has better AUC, but takes longer to run.

4.2 Experiment 2: Graph Classification under IER

In this experiment, we investigate the effects of signal subgraph extraction for later classification. We consider a 3-class classification problem, that is $A|Y = y \sim IER(P^y)$ with $y \in \{0, 1, 2\}$ and

$$P^y = \begin{bmatrix} p^y \times \mathbf{1}_{20 \times 20} & 0.2 \times \mathbf{1}_{20 \times 180} \\ 0.2 \times \mathbf{1}_{180 \times 20} & 0.3 \times \mathbf{1}_{180 \times 180} \end{bmatrix},$$

where

$$p^y = \begin{cases} 0.3 & \text{if } y = 0, \\ 0.4 & \text{if } y = 1, \\ 0.5 & \text{if } y = 2. \end{cases}$$

Based on this data generation scheme, each graph has 200 vertices with the first 20 vertices being the signal vertices. We consider the classification performance of 4 classifiers; specifically, $L(g^*)$, $L(g_V)$, $L(g_S)$, $L(\hat{g}_{\hat{S}})$, where \hat{S} is the estimated signal vertices using one-time screening (\hat{S} -Dcorr, \hat{S} -MGC), or iterative screening (\hat{S} -ItDcorr, \hat{S} -ItMGC). Note that here $L(g^*)$ and $L(g_S)$ are shown for demonstration purpose, which cannot be achieved in practice. With $|S| = 20$, the classification performance and false positive rate in identifying signal vertices are shown in Figure 2. Prediction based on the signal subgraph estimated by the vertex screening has a clear advantage over prediction based on the whole graph. Furthermore, screening with MGC is better than screening with Dcorr, and iterative screening is better than non-iterative screening. Since the setup in this experiment is similar as it in the previous experiment, we do not include CCA or RV here. Note that screening is able to recover the signal vertices perfectly when $m > 300$. However, due to estimation error in \hat{P}^y , $L(\hat{g}_{\hat{S}})$ the prediction error of plugin classifier based on the subgraph is still not as good as Bayes optimal error $L(g^*)$.

If we assume $|S|$ is unknown and estimate the size of signal subgraph via maximizing the distance correlation between the subgraph and label, the resulting subgraph at the maximal correlation statistic coincides with the subgraph of the best classification error. Figure 3 shows the classification error and distance correlation with their standard error for different size of subgraph using iterative screening. Given 300 graphs, finding the best prediction error or maximizing the distance correlation between the subgraph and label yield the same estimate of the size of signal subgraph. However, calculating the distance correlation between subgraph and label is computationally cheaper than computing the

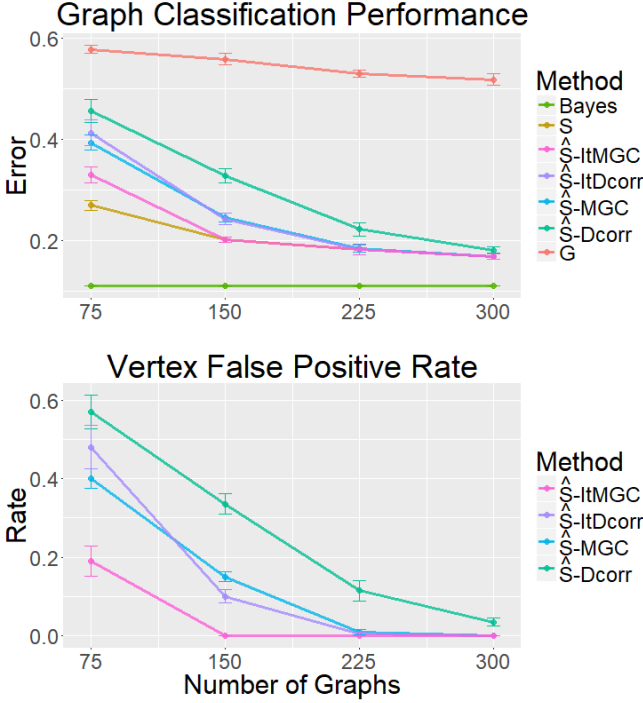


Figure 2: The graph classification error of 7 approaches with their standard errors are shown at the top panel. We generate graphs from 3 inhomogeneous Erdos-Renyi model as described in Section 4.2, then apply 7 approaches to classify these graphs: Bayes plug-in on G (G), Bayes plug-in on $G[\hat{S}]$ (S), Bayes optimal classifier (Bayes), Bayes plug-in on $G[\hat{S}]$ with \hat{S} estimated by Dcorr or MGC (\hat{S} -Dcorr, \hat{S} -MGC), and Bayes plug-in on $G[\hat{S}]$ with \hat{S} estimated by iterative Dcorr or MGC (\hat{S} -ItDcorr, \hat{S} -ItMGC). The plot at top shows prediction error using these 7 approaches. The plot at bottom shows the false positive rate in identifying signal vertices using 4 signal subgraph estimation approaches. The classifiers based on the estimated signal subgraph have significantly better classification performance compared to the classifier based on the whole graph, and are close to Bayes optimal classifier when given 300 graphs. Furthermore, screening with MGC is better than screening with Dcorr and iterative screening is better than non-iterative screening, in terms of both graph classification and signal subgraph estimation.

prediction error. This point will be demonstrated in real data experiments as well.

4.3 Experiment 3: Site and Sex Prediction With Human Functional Magnetic Resonance Images

We consider the task of predicting the site and sex based on functional magnetic resonance image (fMRI) graphs [28]. Two datasets used are SWU4 [29] and HNU1 [30], which have 467 and 300 samples respectively. Each sample is an fMRI scan registered to the MNI152 template using the Desikan atlas, which has 70 regions [31]. We first merge two data sets and then try to predict the site a sample come from. In addition, we try to predict the sex of subject based the fMRI scan.

There are multiple scans (samples) per subject; as a consequence, we carry out a leave-one-subject-out signal

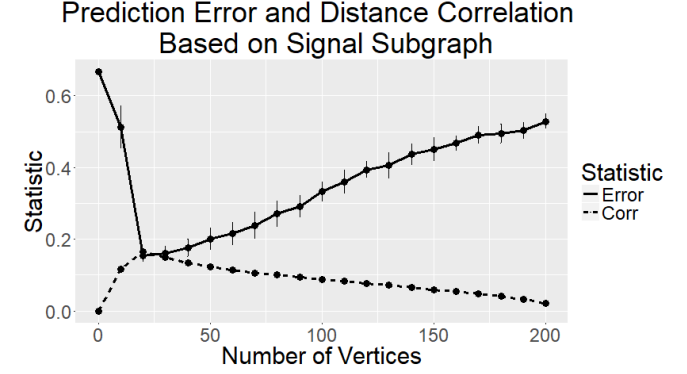


Figure 3: The prediction error and distance correlation with their standard error based on different size of subgraph, produced by the iterative Dcorr screening algorithm. The optimal size of signal subgraph implied by these two statistics are both 20.

subgraph estimation and prediction procedure. To estimate the signal subgraph for site and sex, we first apply iterative vertex screening with samples from one subject left out. Next, we apply 11-Nearest Neighbor to predict the site and sex of the left out samples. The prediction is based on the estimated signal subgraph. This procedure is repeated for all subjects and we compute the leave-one-subject-out screening and prediction error [22], [32].

The prediction error and distance correlation between the subgraph and label with varying size of signal subgraph are shown in Figure 4. Predicting randomly or using no graph at all will have error rate 0.39 and 0.50 for site and sex prediction respectively, which is shown in the Figure 4 with the number of vertices at 0. Sex prediction has prediction error around 0.5 and correlation small. However, the site prediction has achieved high accuracy with classification error less than 0.1 when predicting using a signal subgraph with around 10 – 30 vertices. The best performance is achieved by the signal subgraph with 30 vertices.

As in the simulation experiment, we further utilize the minimum prediction error and the maximum correlation between the subgraph and label to estimate the size of the signal subgraph. In addition, we order the correlations between vertices and the label to find a gap between signal vertices and insignal vertices. The estimated size of signal subgraph to predict site using the three methods is 30, 25 and 27 respectively. The estimated size of signal subgraph to predict sex is 45, 10 and 12. The three different methods yield similar error rate, which validates that the stopping criterion in the iterative screening algorithm works well.

We further apply the iterative vertex screening to all samples and pick the top 30 signal vertices with large distance-based correlations. It turns out that these 30 vertices are matched across left and right hemispheres. If we consider the 35 paired regions in Desikan atlas, we can group the pairs according to whether both regions are among the top 30 signal vertices or not. Table 2 shows the result. The regions with large distance-based correlations are significantly matched based on Chi-square test with a p-value of 0.0020. The 11 left-right hemisphere matched regions are caudal anterior cingulate, corpus callosum,

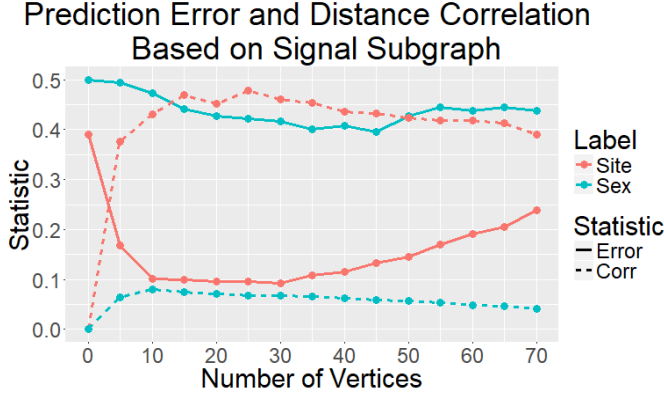


Figure 4: Leave-one-subject-out prediction error and distance correlation based on different size of the signal subgraph. Two studies SWU4 and HNU1 are merged into one data set. We carry out a leave one subject out, screening and prediction procedure to predict sex or site of the left-out sample. The prediction error with different size of signal subgraph is represented by the solid lines. When predicting with no graph or predicting all samples randomly, the prediction error is 0.39 and 0.50 for site and sex respectively, which are shown with the number of vertices being 0. The distance correlation between the subgraph and two covariates is represented by dashed lines. Sex prediction performs poorly in this setting with prediction error being around 0.5 and correlation small. The site prediction has high accuracy with the best performance achieved when the subgraph has 10 – 30 signal vertices.

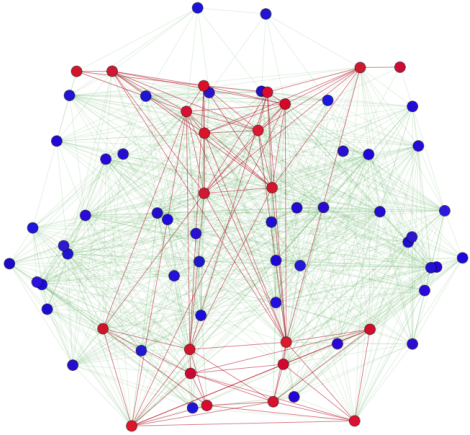


Figure 5: Desikan atlas with highlighted brain regions which are significantly dependent on site. The 11 matched brain regions as found in Table 2 are highlighted in red. They are spatially adjacent.

cuneus, fusiform, lateral occipital, lingual, parsorbitalis, precuneus, rostral anterior cingulate, rostral middle frontal gyrus, and superior frontal gyrus. They are shown in Figure 5.

4.4 Experiment 4: Sex Difference in Mouse Brain with Magnetic Resonance Diffusion Tensor Imaging

Structural magnetic resonance imaging has provided insight into the genetic basis of mouse brain variability, by

	Number of Pairs	Right-Large	Right-Small
Left-Large	11	1	
Left-Small	7		16

TABLE 2: The number of left-right hemisphere matched regions with large or small distance-based correlations.

examining the relationship between volume covariance and genotypes [33]. Using high resolution diffusion tensor imaging and tractography we can now examine the underlying bases for structural connectivity patterns [34], in relationship with genotype and sex. 55 mice brains were scanned and registered into the space of a minimum deformation template, aligned to Waxholm space [35]. The atlas labels were propagated onto the template, and subsequently onto each individual brain using ANTs [36]. DSI Studio [37] was used to estimate tract based structural connectivity for each brain. Each connectome was represented as a graph with 332 vertices, 166 per hemisphere. Out of 55 mice, 32 of them are male and 23 are female. Again, we carry out a leave-one-out iterative vertex screening to estimate the signal subgraph. Then, the left-out sample is predicted based on the estimated signal subgraph using a 9 nearest neighbor classifier. The prediction result and distance correlation based on various size of signal subgraph are shown in Figure 6. Due to the small sample size, the prediction error becomes more volatile. Furthermore, correlation becomes monotone decreasing probably because of over-fitting, since the sample size is small and graph size is large. The iterative screening algorithm yields a signal subgraph of size 10, which is very close to the best possible leave-one-out error at size 20. The top ranked nodes include a thalamic component and the periaqueductal gray, which are important in driving the sexually dimorphic mouse brain development [38] [39].

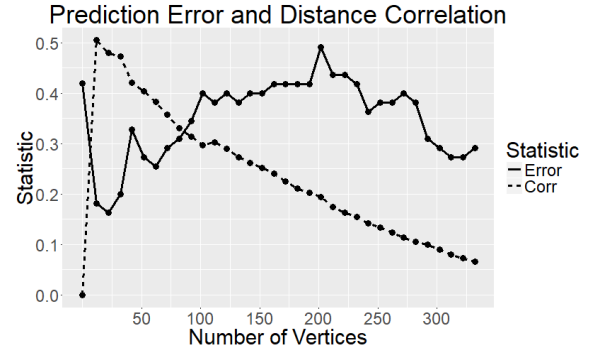


Figure 6: Mouse sex prediction and distance correlation based on different size of signal subgraph. Leave one out iterative vertex screening and prediction is carried on the mouse brain dataset. Signal subgraph with 10 or 20 vertices yield the best performance.

5 DISCUSSION

In summary, we developed an iterative vertex screening methodology to estimate the signal subgraph of interest. The data experiments and theories offer strong evidence that our screening algorithm estimates the signal subgraph effectively and accurately, which leads to better performance

for subsequent inference task. Our approach is intimately related to classical feature screening under linear models [5]–[7]. However, instead of Pearson correlation, we utilize distance correlation [8] and multiscale generalized correlation [11] to measure the dependency between the vertex and response variable. This approach allows the possibility to estimate signal subgraph based on non-scalar response variable or response with non-Euclidean metric. Our method also naturally applies to topological or spectral features of vertices [18], [19], which have been shown to be effective in analyzing fMRI data [40], [41]. Thus our method provides a general and viable tool for supervised learning problems on graphs.

REFERENCES

- [1] E. T. Bullmore and D. S. Bassett, "Brain graphs: graphical models of the human brain connectome," *Annual review of clinical psychology*, vol. 7, pp. 113–140, 2011.
- [2] R. Govindan and H. Tangmunarunkit, "Heuristics for internet map discovery," in *INFOCOM 2000. Nineteenth Annual Joint Conference of the IEEE Computer and Communications Societies. Proceedings. IEEE*, vol. 3. IEEE, 2000, pp. 1371–1380.
- [3] E. Otte and R. Rousseau, "Social network analysis: a powerful strategy, also for the information sciences," *Journal of information Science*, vol. 28, no. 6, pp. 441–453, 2002.
- [4] D. M. Da Zheng, R. Burns, J. Vogelstein, C. E. Priebe, and A. S. Szalay, "Flashgraph: Processing billion-node graphs on an array of commodity ssds," in *Proceedings of the 13th USENIX Conference on File and Storage Technologies*, 2015, pp. 45–58.
- [5] J. Fan and J. Lv, "Sure independence screening for ultrahigh dimensional feature space," *Journal of the Royal Statistical Society: Series B (Statistical Methodology)*, vol. 70, no. 5, pp. 849–911, 2008.
- [6] J. Fan, R. Samworth, and Y. Wu, "Ultrahigh dimensional feature selection: beyond the linear model," *Journal of Machine Learning Research*, vol. 10, no. Sep, pp. 2013–2038, 2009.
- [7] J. Fan, R. Song *et al.*, "Sure independence screening in generalized linear models with np-dimensionality," *The Annals of Statistics*, vol. 38, no. 6, pp. 3567–3604, 2010.
- [8] G. J. Székely, M. L. Rizzo, N. K. Bakirov *et al.*, "Measuring and testing dependence by correlation of distances," *The annals of statistics*, vol. 35, no. 6, pp. 2769–2794, 2007.
- [9] G. J. Székely, M. L. Rizzo *et al.*, "Brownian distance covariance," *The annals of applied statistics*, vol. 3, no. 4, pp. 1236–1265, 2009.
- [10] G. J. Székely and M. L. Rizzo, "The distance correlation t-test of independence in high dimension," *Journal of Multivariate Analysis*, vol. 117, pp. 193–213, 2013.
- [11] C. Shen, C. E. Priebe, M. Maggioni, and J. T. Vogelstein, "Discovering relationships and their structures across disparate data modalities," <https://arxiv.org/abs/1609.05148>, 2017.
- [12] C. Shen, C. E. Priebe, and J. T. Vogelstein, "From distance correlation to multiscale generalized correlation," <https://arxiv.org/abs/1710.09768>, 2017.
- [13] Y. Lee, C. Shen, and J. T. Vogelstein, "Network dependence testing via diffusion maps and distance-based correlations," <https://arxiv.org/abs/1703.10136>, 2017.
- [14] L.-P. Zhu, L. Li, R. Li, and L.-X. Zhu, "Model-free feature screening for ultrahigh-dimensional data," *Journal of the American Statistical Association*, vol. 106, no. 496, pp. 1464–1475, 2011.
- [15] R. Li, W. Zhong, and L. Zhu, "Feature screening via distance correlation learning," *Journal of the American Statistical Association*, vol. 107, no. 499, pp. 1129–1139, 2012.
- [16] L. Devroye, L. Györfi, and G. Lugosi, *A probabilistic theory of pattern recognition*. Springer Science & Business Media, 2013, vol. 31.
- [17] P. Erdős and A. R&WI, "On random graphs i," *Publ. Math. Debrecen*, vol. 6, pp. 290–297, 1959.
- [18] D. L. Sussman, M. Tang, D. E. Fishkind, and C. E. Priebe, "A consistent adjacency spectral embedding for stochastic blockmodel graphs," *Journal of the American Statistical Association*, vol. 107, no. 499, pp. 1119–1128, 2012.
- [19] C. E. Priebe, J. M. Conroy, D. J. Marchette, and Y. Park, "Scan statistics on enron graphs," *Computational & Mathematical Organization Theory*, vol. 11, no. 3, pp. 229–247, 2005.
- [20] D. Cartwright and F. Harary, "Structural balance: a generalization of heider's theory," *Psychological review*, vol. 63, no. 5, p. 277, 1956.
- [21] S. Wang, J. T. Vogelstein, and C. E. Priebe, "Joint embedding of graphs," *arXiv preprint arXiv:1703.03862*, 2017.
- [22] R. Kohavi *et al.*, "A study of cross-validation and bootstrap for accuracy estimation and model selection," in *Ijcai*, vol. 14, no. 2. Stanford, CA, 1995, pp. 1137–1145.
- [23] M. Zhu and A. Ghodsi, "Automatic dimensionality selection from the scree plot via the use of profile likelihood," *Computational Statistics & Data Analysis*, vol. 51, no. 2, pp. 918–930, 2006.
- [24] H. Hotelling, "Relations between two sets of variates," *Biometrika*, vol. 28, no. 3/4, pp. 321–377, 1936.
- [25] P. Robert and Y. Escoufier, "A unifying tool for linear multivariate statistical methods: the rv-coefficient," *Applied statistics*, pp. 257–265, 1976.
- [26] J. A. Hanley and B. J. McNeil, "The meaning and use of the area under a receiver operating characteristic (roc) curve," *Radiology*, vol. 143, no. 1, pp. 29–36, 1982.
- [27] T. Fawcett, "An introduction to roc analysis," *Pattern recognition letters*, vol. 27, no. 8, pp. 861–874, 2006.
- [28] S. Ogawa, T.-M. Lee, A. R. Kay, and D. W. Tank, "Brain magnetic resonance imaging with contrast dependent on blood oxygenation," *Proceedings of the National Academy of Sciences*, vol. 87, no. 24, pp. 9868–9872, 1990.
- [29] J. Qiu, Z. Qinglin, T. Bi, G. Wu, D. Wei, and W. Yang, "Southwest university longitudinal imaging multimodal (slim) brain data repository: A long-term test-retest sample of young healthy adults in southwest china." [Online]. Available: <http://dx.doi.org/10.15387/fcpindi.retro.slim>
- [30] X. Weng and X. Zuo, "One-month test-retest reliability and dynamical resting-state study." [Online]. Available: <http://dx.doi.org/10.15387/fcpindi.corr.hnu1>
- [31] R. S. Desikan, F. Ségonne, B. Fischl, B. T. Quinn, B. C. Dickerson, D. Blacker, R. L. Buckner, A. M. Dale, R. P. Maguire, B. T. Hyman *et al.*, "An automated labeling system for subdividing the human cerebral cortex on mri scans into gyral based regions of interest," *Neuroimage*, vol. 31, no. 3, pp. 968–980, 2006.
- [32] T. Cover and P. Hart, "Nearest neighbor pattern classification," *IEEE transactions on information theory*, vol. 13, no. 1, pp. 21–27, 1967.
- [33] A. Badea, G. A. Johnson, and R. Williams, "Genetic dissection of the mouse brain using high-field magnetic resonance microscopy," *Neuroimage*, vol. 45, no. 4, pp. 1067–1079, 2009.
- [34] E. Calabrese, A. Badea, G. Cofer, Y. Qi, and G. A. Johnson, "A diffusion mri tractography connectome of the mouse brain and comparison with neuronal tracer data," *Cerebral Cortex*, vol. 25, no. 11, pp. 4628–4637, 2015.
- [35] G. A. Johnson, A. Badea, J. Brandenburg, G. Cofer, B. Fubara, S. Liu, and J. Nissanov, "Waxholm space: an image-based reference for coordinating mouse brain research," *Neuroimage*, vol. 53, no. 2, pp. 365–372, 2010.
- [36] B. B. Avants, N. J. Tustison, G. Song, P. A. Cook, A. Klein, and J. C. Gee, "A reproducible evaluation of ants similarity metric performance in brain image registration," *Neuroimage*, vol. 54, no. 3, pp. 2033–2044, 2011.
- [37] F.-C. Yeh, T. D. Verstynen, Y. Wang, J. C. Fernández-Miranda, and W.-Y. I. Tseng, "Deterministic diffusion fiber tracking improved by quantitative anisotropy," *PLoS one*, vol. 8, no. 11, p. e80713, 2013.
- [38] S. Spring, J. P. Lerch, and R. M. Henkelman, "Sexual dimorphism revealed in the structure of the mouse brain using three-dimensional magnetic resonance imaging," *Neuroimage*, vol. 35, no. 4, pp. 1424–1433, 2007.
- [39] A. Raznahan, F. Probst, M. R. Palmert, J. N. Giedd, and J. P. Lerch, "High resolution whole brain imaging of anatomical variation in xo, xx, and xy mice," *Neuroimage*, vol. 83, pp. 962–968.
- [40] Q. K. Telesford, A. R. Morgan, S. Hayasaka, S. L. Simpson, W. Barrett, R. A. Kraft, J. L. Mozolic, and P. J. Laurienti, "Reproducibility of graph metrics in fmri networks," *Frontiers in neuroinformatics*, vol. 4, 2010.
- [41] R. Tang, M. Ketcha, J. T. Vogelstein, C. E. Priebe, and D. L. Sussman, "Law of large graphs," *arXiv preprint arXiv:1609.01672*, 2016.
- [42] W. Hoeffding, "Probability inequalities for sums of bounded random variables," *Journal of the American statistical association*, vol. 58, no. 301, pp. 13–30, 1963.

APPENDICES

5.1 Review on Distance Correlation and Multiscale Generalized Correlation

The distance correlation (Dcorr) [8], [9] and multiscale generalize correlation (MGC) [11], [12] are two correlation measures for dependency between any two random variables $X \in \mathbb{R}^p$ and $Y \in \mathbb{R}^q$. The distance covariance $Dcov(X, Y)$ is given by

$$Dcov(X, Y) = \frac{1}{c_p c_q} \iint \frac{|\phi_{X,Y}(s, t) - \phi_X(s)\phi_Y(t)|^2}{\|s\|^{1+p}\|t\|^{1+q}} dt ds, \quad (1)$$

where $\phi_{X,Y}$, ϕ_X and ϕ_Y are characteristic functions of (X, Y) , X and Y respectively, and c_p, c_q are constants. When X and Y have finite second moment, it can be shown that the distance correlation can be alternatively defined by

$$Dcov(X, Y) = \mathbb{E}(\|X - X'\| \|Y - Y'\|) + \mathbb{E}(\|X - X'\|) \mathbb{E}(\|Y - Y'\|) - 2\mathbb{E}(\|X - X'\| \|Y - Y''\|),$$

where $(X, Y), (X', Y'), (X'', Y'')$ are independent and identically distributed as F_{XY} . Distance covariance between two random variables X and Y is always non-negative, and it equals 0 if and only if X and Y are independent. The distance correlation $Dcorr(X, Y)$ between X and Y is

$$Dcorr(X, Y) = \frac{Dcov(X, Y)}{\sqrt{Dcov(X, X) Dcov(Y, Y)}},$$

which lies in $[0, 1]$.

When applying distance correlation to sample data, the sample distance correlation is defined by properly centering Euclidean distance matrices, followed by taking a Hadamard product. The sample Dcorr converges to the population Dcorr as sample size increases to infinity, therefore we concentrate on analyzing the population Dcorr in the theoretical proofs.

The more recent multiscale generalized correlation (MGC) is a local optimal version of distance correlation: when evaluating the integral in Equation (1), the characteristic function is truncated to a neighborhood, which can be shown to yield a larger statistic and better test power under a wide variety of high-dimensional and non-linear dependence cases. A detailed discussion of MGC is in [12], which essentially shares the same theoretical properties as distance correlation.

Proof of Lemma 3.2

By definition of distance covariance,

$$\begin{aligned} Dcov(X, Y) &= \frac{1}{c_{p+r} c_q} \int_{s,t} \frac{|\phi_{X,Y}(s, t) - \phi_X(s)\phi_Y(t)|^2}{\|s\|^{1+p+r}\|t\|^{1+q}} \\ &= \frac{1}{c_{p+r} c_q} \int_{s_p, s_r, t} \frac{|\phi_{X^*,Y}(s_p, t) - \phi_{X^*}(s_p)\phi_Y(t)|^2 |\phi_Z(s_r)|^2}{\|[s_p, s_r]\|^{1+p+r}\|t\|^{1+q}} \\ &\leq \frac{1}{c_{p+r} c_q} \int_{s_p, s_r, t} \frac{|\phi_{X^*,Y}(s_p, t) - \phi_{X^*}(s_p)\phi_Y(t)|^2}{\|[s_p, s_r]\|^{1+p+r}\|t\|^{1+q}} \\ &= Dcov([X^*, \vec{0}], Y), \end{aligned}$$

where the inequality holds because $|\phi_Z(s_r)| \leq 1$.

Using the alternative definition of distance covariance, we have

$$\begin{aligned} Dcov([X^*, \vec{0}], Y) &= \mathbb{E}(\|X^*, \vec{0}\|) - \mathbb{E}(\|X^*, \vec{0}\|) \mathbb{E}(\|Y - Y'\|) \\ &\quad + \mathbb{E}(\|X^*, \vec{0}\|) \mathbb{E}(\|Y - Y'\|) \mathbb{E}(\|Y - Y''\|) \\ &\quad - 2\mathbb{E}(\|X^*, \vec{0}\|) \mathbb{E}(\|Y - Y''\|) \\ &= \mathbb{E}(\|X^* - X^{*'}\| \|Y - Y'\|) \\ &\quad + \mathbb{E}(\|X^* - X^{*'}\|) \mathbb{E}(\|Y - Y'\|) \\ &\quad - 2\mathbb{E}(\|X^* - X^{*'}\|) \mathbb{E}(\|Y - Y''\|) \\ &= Dcov(X^*, Y). \end{aligned}$$

This concludes $Dcov(X^*, Y) \geq Dcov(X, Y)$.

Proof of Theorem 3.3

By definition of distance correlation,

$$Dcorr(X_r, Y) = \frac{Dcov(X_r, Y)}{\sqrt{Dcov(X_r, X_r) Dcov(Y, Y)}}.$$

We first show that $Dcov(X_r, Y)$ converges to 0 as the number of noise dimension r goes to infinity. By definition,

$$\begin{aligned} Dcov(X_r, Y) &= \mathbb{E}(\|X_r - X'_r\| \|Y - Y'\|) + \\ &\quad \mathbb{E}(\|X_r - X'_r\|) \mathbb{E}(\|Y - Y'\|) - 2\mathbb{E}(\|X_r - X'_r\| \|Y - Y''\|) \\ &= \mathbb{E}(\|X_r - X'_r\| \|Y - Y'\|) - \mathbb{E}(\|X_r - X'_r\|) \mathbb{E}(\|Y - Y'\|) + \\ &\quad 2\mathbb{E}(\|X_r - X'_r\|) \mathbb{E}(\|Y - Y'\|) - 2\mathbb{E}(\|X_r - X'_r\| \|Y - Y''\|) \\ &= Cov(\|X_r - X'_r\|, \|Y - Y'\|) \\ &\quad - 2Cov(\|X_r - X'_r\|, \|Y - Y''\|) \end{aligned}$$

Let us look at $Cov(\|X_r - X'_r\|, \|Y - Y'\|)$.

$$\begin{aligned} Cov(\|X_r - X'_r\|, \|Y - Y'\|) &= \mathbb{E}(\|X_r - X'_r\| \|Y - Y'\|) - \mathbb{E}(\|X_r - X'_r\|) \mathbb{E}(\|Y - Y'\|) \\ &\leq \mathbb{E}(\|X_r - X'_r\| \|Y - Y'\|) - \mathbb{E}(\|Z_r - Z'_r\|) \mathbb{E}(\|Y - Y'\|) \\ &= \mathbb{E}(\|X_r - X'_r\| \|Y - Y'\|) - \mathbb{E}(\|Z_r - Z'_r\| \|Y - Y'\|) \\ &= \mathbb{E}(\|X_r - X'_r\| \|Y - Y'\| - \|Z_r - Z'_r\| \|Y - Y'\|) \end{aligned}$$

Let Z be the first entry of Z_r , and we define

$$\begin{aligned} \mu &= \mathbb{E}((Z - Z')^2), \\ \sigma^2 &= Var((Z - Z')^2), \\ \gamma^2 &= Cov((Z - Z')^2, (Z - Z'')^2). \end{aligned}$$

Applying the Taylor expansion to $\sqrt{\frac{\|Z_r - Z'_r\|^2}{r}}$ at μ , we have

$$\begin{aligned} \frac{\|Z_r - Z'_r\|}{\sqrt{r}} &= \mu^{\frac{1}{2}} + \frac{1}{2}\mu^{-\frac{1}{2}}\left(\frac{\|Z_r - Z'_r\|^2}{r} - \mu\right) \\ &\quad - \frac{1}{8}\left(\frac{\|Z_r - Z'_r\|^2}{r} - \mu\right)^2 + O(r^{-\frac{3}{2}}). \end{aligned}$$

Similarly,

$$\begin{aligned} \frac{\|X_r - X'_r\|}{\sqrt{r}} &= \mu^{\frac{1}{2}} + \frac{1}{2}\mu^{-\frac{1}{2}}\left(\frac{\|X_r - X'_r\|^2}{r} - \mu\right) \\ &\quad - \frac{1}{8}\left(\frac{\|X_r - X'_r\|^2}{r} - \mu\right)^2 + O(r^{-\frac{3}{2}}). \end{aligned}$$

Therefore,

$$\|X_r - X'_r\| - \|Z_r - Z'_r\| = O(r^{-\frac{1}{2}}).$$

As a consequence,

$$\begin{aligned} & \text{Cov}(\|X_r - X'_r\|, \|Y - Y'\|) \\ & \leq \mathbb{E}(\|X_r - X'_r\| \|Y - Y'\| - \|Z_r - Z'_r\| \|Y - Y'\|) \\ & = O(r^{-\frac{1}{2}}). \end{aligned}$$

We can also derive a lower bound:

$$\begin{aligned} & \text{Cov}(\|X_r - X'_r\|, \|Y - Y'\|) \\ & = \mathbb{E}(\|X_r - X'_r\| \|Y - Y'\|) - \mathbb{E}(\|X_r - X'_r\|) \mathbb{E}(\|Y - Y'\|) \\ & \geq \mathbb{E}(\|Z_r - Z'_r\| \|Y - Y'\|) - \mathbb{E}(\|X_r - X'_r\|) \mathbb{E}(\|Y - Y'\|) \\ & = \mathbb{E}(\|Z_r - Z'_r\|) \mathbb{E}(\|Y - Y'\|) - \mathbb{E}(\|X_r - X'_r\|) \mathbb{E}(\|Y - Y'\|) \\ & = \mathbb{E}(\|Z_r - Z'_r\| - \|X_r - X'_r\|) \mathbb{E}(\|Y - Y'\|) \\ & = O(r^{-\frac{1}{2}}) \end{aligned}$$

Similarly, we can show that

$$\text{Cov}(\|X_r - X'_r\|, \|Y - Y''\|) \rightarrow 0.$$

This proves $D\text{cov}(X_r, Y) \rightarrow 0$.

Next, we demonstrate that $D\text{cov}(X_r, X_r)$ is non-vanishing. Again, we need to analyze $\text{Cov}(\|X_r - X'_r\|, \|X_r - X''_r\|)$ and $\text{Cov}(\|X_r - X'_r\|, \|X_r - X''_r\|)$.

$$\begin{aligned} & \text{Cov}(\|X_r - X'_r\|, \|X_r - X''_r\|) \\ & = \mathbb{E}(\|X_r - X'_r\|^2) - \mathbb{E}^2(\|X_r - X'_r\|) \\ & = \mathbb{E}(\|X^* - X^{*\prime}\|^2) + r\mu - \mathbb{E}^2(\|X_r - X'_r\|) \\ & = \mathbb{E}(\|X^* - X^{*\prime}\|^2) + r\mu - \\ & \quad r(\mu^{\frac{1}{2}} + \frac{1}{2}\mu^{-\frac{1}{2}}\frac{\mathbb{E}(\|X^* - X^{*\prime}\|^2)}{r} - \frac{1}{8}\mu^{-\frac{3}{2}}\frac{\sigma^2}{r} + O(r^{-\frac{3}{2}}))^2 \\ & = \frac{1}{4}\mu^{-1}\sigma^2 + O(r^{-1}). \end{aligned}$$

Use the similar Taylor expansion technique, we can show

$$\text{Cov}(\|X_r - X'_r\|, \|X_r - X''_r\|) = \frac{1}{8}\mu^{-1}\gamma^2 + O(r^{-1}).$$

As long as Z is non-degenerate, $\sigma^2 - \gamma^2 > 0$. This shows

$$\lim_{r \rightarrow \infty} D\text{cov}(X_r, X_r) = \frac{1}{4}\mu^{-1}(\sigma^2 - \gamma^2) > 0$$

Moreover, $D\text{cov}(Y, Y)$ is always a fixed positive number for non-degenerate Y , thus we conclude

$$\lim_{r \rightarrow \infty} D\text{corr}(X_r, Y) = 0.$$

Proof of Theorem 3.4

It suffices to show the Bayes plug-in density $\mathcal{L}(A; \hat{P}^y)$ is close to the true density $\mathcal{L}(A; P^y)$ with high probability. We will assume $\pi_y \geq \alpha$ for some fixed $\alpha > 0$. Applying Hoeffding's Equality to $\hat{\pi}_y$ [42],

$$\mathbb{P}(|\hat{\pi}_y - \pi_y| < \epsilon_1) \geq 1 - 2 \exp(-2m\epsilon_1^2).$$

By choosing ϵ_1 small enough such that $\hat{\pi}_y > \frac{\alpha}{2}$, and applying Hoeffding's Equality to \hat{P}_{ij}^y , it follows that

$$\mathbb{P}(|\hat{P}_{ij}^y - P_{ij}^y| < \epsilon_2) \geq 1 - 2 \exp(-m\alpha\epsilon_2^2).$$

If $|\hat{\pi}_y - \pi_y| < \epsilon_1$ and $|\hat{P}_{ij}^y - P_{ij}^y| < \epsilon_2$, for any adjacency matrix A :

$$\begin{aligned} & |\pi_y \mathcal{L}(A; P^y) - \hat{\pi}_y \mathcal{L}(A; \hat{P}^y)| \\ & \leq |\pi_y \mathcal{L}(A; \hat{P}^y) - \hat{\pi}_y \mathcal{L}(A; \hat{P}^y)| \\ & \quad + |\pi_y \mathcal{L}(A; P^y) - \pi_y \mathcal{L}(A; \hat{P}^y)| \\ & < \epsilon_1 + |\pi_y \mathcal{L}(A; P^y) - \pi_y \mathcal{L}(A; \hat{P}^y)| \\ & < \epsilon_1 + |\mathcal{L}(A; P^y) - \mathcal{L}(A; \hat{P}^y)| \\ & < \epsilon_1 + e\epsilon_2. \end{aligned}$$

The last inequality follows from recursively applying the technique used in the first inequality and the fact that $|\hat{P}_{ij}^y - P_{ij}^y| < \epsilon_2$. As a consequence, conditioned on $\hat{\pi}_y$ and \hat{P}^y satisfy the Hoeffding's inequality,

$$\begin{aligned} & |\mathbb{E}_A(|\pi_0 \mathcal{L}(A; P^0) - \hat{\pi}_0 \mathcal{L}(A; \hat{P}^0)| \\ & \quad + |\pi_1 \mathcal{L}(A; P^1) - \hat{\pi}_1 \mathcal{L}(A; \hat{P}^1)|)| \leq 2(\epsilon_1 + e\epsilon_2). \end{aligned}$$

Setting $2(\epsilon_1 + e\epsilon_2) = \epsilon$ and $2\epsilon_1^2 = \alpha\epsilon_2^2$, we have $\epsilon_2 = \frac{\epsilon}{2e + \sqrt{2\alpha}}$. Then, apply Theorem 2.3 in [16] yields

$$\mathbb{P}(L(g_V) - L(g^*) < \epsilon) \geq 1 - 2(e+1) \exp\left(\frac{-m\alpha\epsilon^2}{(2e + \sqrt{2\alpha})^2}\right).$$

Alternatively, setting $\eta = 2(e+1) \exp\left(\frac{-m\alpha\epsilon^2}{(2e + \sqrt{2\alpha})^2}\right)$ yields that with probability at least $1 - \eta$, it holds that

$$L(g_V) - L(g^*) \leq (2e + \sqrt{2\alpha}) \sqrt{\frac{\log\left(\frac{2(e+1)}{\eta}\right)}{m\alpha}}.$$

Proof of Corollary 3.5

Following Theorem 3.2, we have

$$\begin{aligned} & \mathbb{E}(L(g_V)) - L(g^*) \\ & = \mathbb{E}(L(g_V) - L(g^*)) \\ & < \epsilon \mathbb{I}\{L(g_V) - L(g^*) < \epsilon\} + \mathbb{I}\{L(g_V) - L(g^*) \geq \epsilon\} \\ & < \epsilon + 2(e+1) \exp\left(\frac{-m\alpha\epsilon^2}{(2e + \sqrt{2\alpha})^2}\right). \end{aligned}$$